The Astrophysical Journal Letters, 830:L29 (5pp), 2016 October 20 doi:10.3847/2041-8205/830/2/L29

THE IMPACT EJECTA ENVIRONMENT OF NEAR EARTH ASTEROIDS

Jamey R. Szalay[1] and Mihály Horányi[2,3,4]
[1] Southwest Research Institute, 6220 Culebra Rd, San Antonio, TX 78238, USA
[2] Department of Physics, University of Colorado Boulder, 392 UCB, Boulder, CO 80309, USA
[3] Laboratory for Atmospheric and Space Physics,1234 Innovation Dr., Boulder, CO 80303,USA
[4] Institute for Modeling Plasma, Atmospheres, and Cosmic Dust, 3400 Marine St., Boulder, CO 80303, USA
Received 2016 September 8; revised 2016 October 3; accepted 2016 October 4; published 2016 October 18

ABSTRACT

Impact ejecta production is a ubiquitous process that occurs on all airless bodies throughout the solar system. Unlike the Moon, which retains a large fraction of its ejecta, asteroids primarily shed their ejecta into the interplanetary dust population. These grains carry valuable information about the chemical compositions of their parent bodies that can be measured via in situ dust detection. Here, we use recent *Lunar Atmosphere and Dust Environment Explorer*/Lunar Dust Experiment measurements of the lunar dust cloud to calculate the dust ejecta distribution for any airless body near 1 au. We expect this dust distribution to be highly asymmetric, due to non-isotropic impacting fluxes. We predict that flybys near these asteroids would collect many times more dust impacts by transiting the apex side of the body compared to its anti-apex side. While these results are valid for bodies at 1 au, they can be used to qualitatively infer the ejecta environment for all solar-orbiting airless bodies.

Key words: meteorites, meteors, meteoroids – minor planets, asteroids: general – zodiacal dust

1. INTRODUCTION

The Lunar Dust Experiment (LDEX; Horányi et al. 2014) on board the *Lunar Atmosphere and Dust Environment Explorer* mission (Elphic et al. 2014) took measurements of the lunar dust cloud from 2013 October to 2014 April. LDEX observed an asymmetric dust density distribution (Horányi et al. 2015) sustained primarily by the helion (HE), apex (AP), and anti-helion (AH) sporadic meteoroid sources (Szalay & Horányi 2015a), with a minor contribution potentially coming from the anti-apex (AA) source (Szalay & Horányi 2016b). During many of the known meteoroid showers, the dust density was observed to significantly increase on the hemisphere impacted by the meteoroid stream (Szalay & Horányi 2016a).

Just like the Earth-Moon system, asteroids are constantly barraged by meteoroids. When a meteoroid impacts the surface of an airless body, it ejects orders of magnitude more material than the primary impactor. The moon's gravity traps the large majority of these ejecta particles, as was measured by LDEX. However, asteroids, due to their diminished gravity, are expected to shed most of these particles, spawning more meteoroids into the population of interplanetary dust particles in the solar system.

Near Earth Objects (NEOs) are bodies with aphelia $Q \geqslant 0.983$ au and perihelia $q < 1.3$ au (Bottke et al. 2002). For this study, we focus on dust production from Near Earth Asteroids (NEA), as the number of comets in the total NEO population is significantly less than the number of NEAs (Harris & D'Abramo 2015). The number of NEOs with radii $R \gtrsim 10$ km is estimated to range from a few to ten (Mainzer et al. 2011; Harris & D'Abramo 2015).

We use the measured dust flux at the Moon to investigate the dust ejecta from much smaller bodies at 1 au that experience a similar influx of bombarding meteoroids. We focus on NEAs, as they are expected to experience a nearly identical flux as the Moon, allowing for a direct analogy to be made between the two types of ejecta clouds. In Section 2 we calculate the ejecta density distributions for these bodies as a function of their sizes. In Section 3, we investigate the flux of escaping dust particles that a spacecraft would be exposed to during close flybys. In Section 4, we conclude with a discussion of the applicability of our estimates to other airless bodies in the solar system.

2. EJECTA FROM AIRLESS BODIES NEAR 1 au

The initial velocity distribution function for dust grains ejected from the lunar surface was determined to have the form

$$f(\hat{v}) = \frac{\delta \hat{v}}{(1-\hat{v}^2)^2} e^{-\frac{\beta \hat{v}}{1-\hat{v}^2}}, \quad (1)$$

where $\hat{v} = v/v_m$ with $v_m = 2.4\,\mathrm{km\,s^{-1}}$ (lunar escape speed), $\beta = 8.69$, and $\delta = 7.2 \times 10^{-3}\,\mathrm{s\,m^{-1}}$ (Szalay & Horányi 2016b). This distribution was derived assuming LDEX only detected bound grains at their turning points; it therefore represents an approximation of $f(\hat{v})$ at the Moon. Assuming that the large majority of grains ejected from the lunar surface are non-escaping, and that thus $f(\hat{v})$ approximates the true velocity distribution, we take $f(\hat{v})$ to be representative of the initial velocity distribution for all airless regolith bodies at 1 au and use it to derive the dust density distribution around these bodies. While $f(\hat{v})$ describes a gravitationally bound ejecta cloud at the Moon, it indicates that the vast majority of the dust particles escape from NEAs.

For a body of radius R, the dust production rate as a function of φ, the angle from apex, and grain size a is $Q(\varphi, a) = 4\pi R^2 F(\varphi, a)$, where F is the outgoing flux. At the Moon, the ejecta cloud was observed to be highly asymmetric (Szalay & Horányi 2015a, 2016b). The very same sources that produce the majority of lunar dust ejecta (HE, AP, AH, AA) are expected to produce a similarly asymmetric dust cloud around asteroids. Using the ejecta distribution observed at the Moon, the ejecta flux is,

$$F(\varphi, a) = F_w a_\mu^{-2.7} \sum_s w_s \cos^3(\varphi - \varphi_s)\Theta(\varphi_s - \pi/2), \quad (2)$$

where a_μ is the particle radius in μm, s represents each source, Θ is the Heaviside function, φ_s is the characteristic angle for

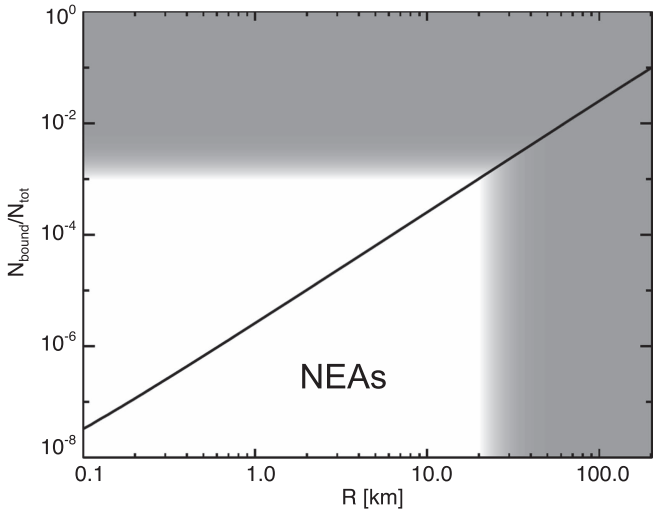

Figure 1. Fraction of bound grains to total ejected grains, where $N_{\rm bound}/N_{\rm tot} = \int_0^{v_e} f(\hat{v})dv$. For the largest observed NEAs ($R \approx 10$–20 km), more than 99.9% of all grains ejected with $f(\hat{v})$ in Equation (1) are unbound.

each of the four source radiants (65°, 0°, −65°, 180°) (Campbell-Brown 2008), $F_w = 0.22\,{\rm m}^{-2}\,{\rm s}^{-1}$, and w_s is the relative weight (0.24, 0.49, 0.24, 0.03) for the HE, AP, AH, & AA sources, respectively. The relative ratios of AP to HE/AH sources are taken from a synthesis of ground-based radar measurements at Earth (Campbell-Brown 2008) and dust measurements at the Moon (Szalay & Horányi 2016b). We take the cumulative particle size distribution of $f(>a) \propto a^{-2.7}$ measured at the Moon (Horányi et al. 2015) to be applicable to all regolith bodies. From energy conservation, we calculate the ratio of bound grains to total ejecta as a function of R (Figure 1). For the largest observed NEAs ($R \approx 10$–20 km), approximately 99.9% of all grains ejected with $f(\hat{v})$ in Equation (1) are unbound.

Conserving the number of particles and assuming that grains are ejected with velocities $v \gg v_e$, where v_e is the escape velocity of the body, the number density as a function of radial distance r from the body is $n(r, \varphi, a) = Q(\varphi, a)/4\pi v r^2$. Integrating this over the entire velocity distribution yields

$$n(r, \varphi, a) = \delta F(\varphi, a)\left(\frac{R}{r}\right)^2 \underbrace{\int_0^1 \frac{e^{-\frac{\beta\hat{v}^2}{1-\hat{v}^2}}}{(1-\hat{v}^2)^2}\,d\hat{v}}_{I \approx 0.31}. \quad (3)$$

The lower bound of the integral in Equation (3) is approximately 0 in the regime where $v_e \ll v \ll v_m$. Combining Equations (2) and (3), the complete average dust density distribution is

$$n(r, \varphi, a) = n_w \left(\frac{R}{r}\right)^2 a_\mu^{-2.7} \times \sum_s w_s \cos^3(\varphi - \varphi_s)\Theta(\varphi_s - \pi/2), \quad (4)$$

where $n_w = \delta F_w I = 4.9 \times 10^{-4}$ m^{-3}. Figure 2 shows this density distribution for $a \geqslant 0.3\,\mu$m and $R = 10$ km. The particle size threshold of $a \geqslant 0.3\,\mu$m is the minimum particle size able to be individually detected by LDEX at the Moon.

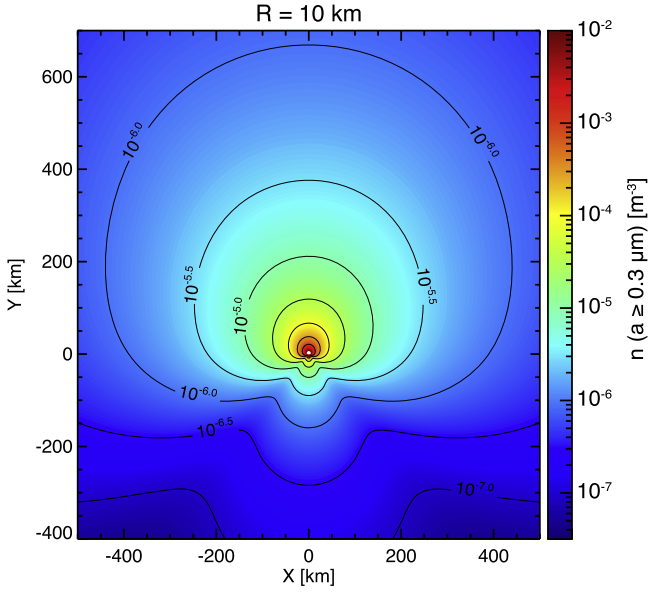

Figure 2. Dust density distribution in the ecliptic frame for grains with $a \geqslant 0.3\,\mu$m above a body with $R = 10$ km. The apex is in the $+y$ direction.

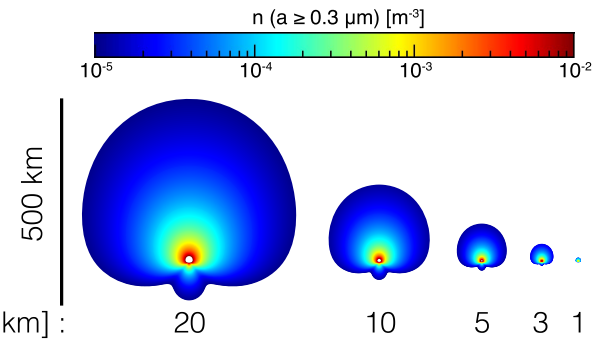

Figure 3. Dust density distribution for grains with $a \geqslant 0.3\,\mu$m in the ecliptic frame for selected asteroid sizes. The scale of the dust cloud size is proportional to R^2.

Since the size distribution for lunar ejecta has been verified for sizes at and above this value, we use this as the canonical value for the remainder of this analysis. Additionally, we employ $R = 10$ km as the body size for the majority of calculated quantities, as this is on the upper end of detected NEAs and will sustain some of the most dense dust clouds for NEAs.

The density distribution is highly asymmetric with respect to the apex direction ($+y$ in Figure 2). The main sources found to produce dust at the Moon are the HE, AP, and AH sources, all of which are concentrated on the apex hemisphere. The last source, AA, was introduced to fit the non-zero dust density measured by LDEX at lunar dusk (Szalay & Horányi 2016b). The statistics were not sufficient to constrain its contribution in the same manner as the other three sources and a relative ratio of $w_{\rm AA} = 3\%$ was chosen as a reasonable value. Because the exact value of this mixing ratio remains poorly constrained, other than that it must be small and non-zero, the substructure depicted on the anti-apex hemisphere in Figure 2 represents a more qualitative estimate of the true dust distribution than at other local times.

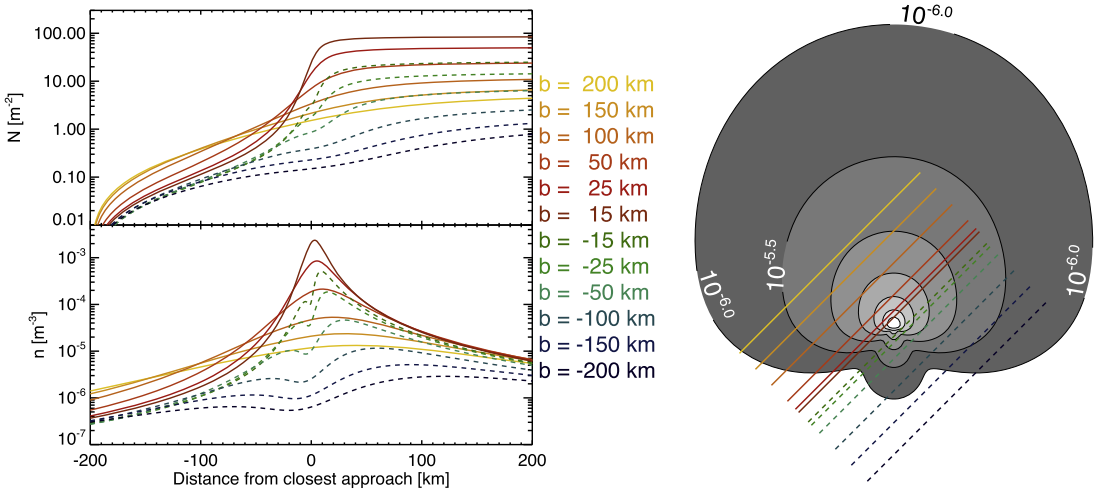

Figure 4. Total number of impacts per square meter and predicted dust density ($a \geqslant 0.3$ μm) for spacecraft flybys as a function of distance from the closest approach and impact parameter (b) for a body with $R = 10$ km. Contours are logarithmically spaced in half decades of m^{-3}.

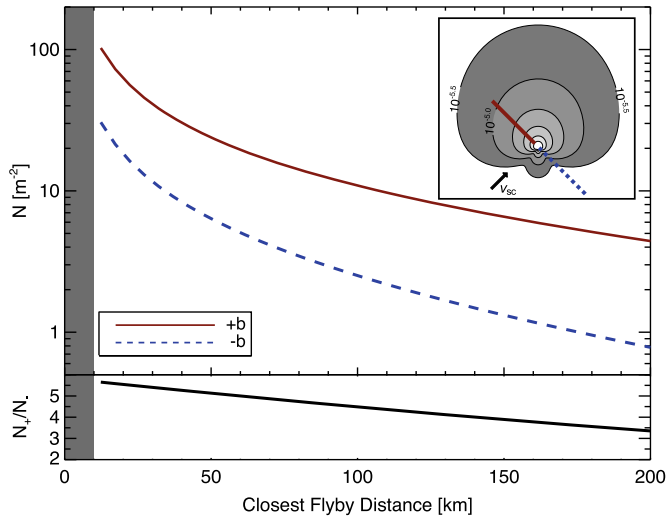

Figure 5. Total number of impacts per square meter ($a \geqslant 0.3$ μm) for spacecraft flybys as a function of impact parameter for a body with $R = 10$ km. The two curves show the discrepancy between flying on the apex (solid line) or anti-apex (dashed line) sides, with their ratios shown in the bottom panel. The gray bar from 0 to 10 km indicates the radius of the body. The inset depicts the geometry of the closest flyby distances, where the contours are given in m^{-3} and the arrow indicates the direction of spacecraft motion used for the calculation.

Figure 3 shows the relative size of asteroidal dust clouds as a function of body radius. Since the total amount of ejecta is a function of the exposed surface area, larger bodies have significantly denser dust clouds than smaller bodies, as the asteroidal gravity remains negligible in dictating the dust distribution due to the fact that the large majority of grains are ejected well above escape speeds.

3. SPACECRAFT MEASUREMENTS

A useful quantity for scientific and/or hazard-driven studies is the impact rate that a spacecraft would experience during a flyby of an NEA. Since the ejecta distribution is highly asymmetric, the impact rate profile depends on the trajectory geometry. As an example, we investigate the family of trajectories that transit the ejecta cloud at an angle of 45° with respect to the apex direction.

To determine the total number of impacts experienced by a spacecraft with a close flyby of an NEA, we integrate the density along straight trajectories with the closest approach distance b from the center of the asteroid. As in the previous section, we use $R = 10$ km for the following analysis. Figure 4 shows a selection of these trajectories for $b = 15$, 25, 50, 100, 150, and 200 km, where the minus sign on b is used to distinguish trajectories that transit the apex (+) and anti-apex (−) hemispheres. The majority of impacts occur within tens of kilometers from the closest approach. As shown in Figure 4, the asymmetric dust cloud leads to an asymmetric impact rate distribution between the two sets of trajectories. Figure 5 shows the total counts per unit area as a function of b. For close flybys (less than a few tens of kilometers), apex side trajectories attain a factor of ∼5 larger total number of impacts than the corresponding anti-apex trajectory. For flybys at large altitudes (∼100 km), this ratio decreases to ∼3.

A spacecraft performing flybys of these asteroids equipped with a dust detector would need to consider additional constraints. For impact ionization dust detectors, particularly those with chemical composition capability (Postberg et al. 2011), the relative impact velocity between dust grains and the detector must be sufficiently large (∼a few km s^{-1}). Such an instrument could sample the chemical composition of the asteroidal surface without landing on the target body. The minimum detectable size is a function of impact velocity, typically a power law in velocity for impact ionization dust detectors. For the $R = 10$ km case discussed throughout this work, and a minimum detectable grain size of 0.3 μm, a detector would experience on the order of tens of impacts per m^2. This total count rate scales as $R^2 a^{-2.7}$, which significantly reduces the expected impact rates for smaller bodies. Table 1 gives the expected number of counts for a 1 and 10 km body. Flybys of objects with $R < 10$ km are not expected to be suitable for in situ dust detector observations.

To make realistic predictions of the detectable impact rates for future missions, the true spacecraft trajectory has to be incorporated in the analysis combined with the size/speed-dependent thresholds of a dust detector. However, a spacecraft equipped with an aerogel collector similar to that of the Stardust mission (Westphal et al. 2004) could directly capture asteroidal ejecta particles for subsequent analysis following the sample's return to Earth.

Table 1
Total Impacts for Selected Flyby Parameters

	$R = 1$ km		$R = 10$ km	
$a_{\min}$ (μm)	$b = 15$ km	$b = 100$ km	$b = 15$ km	$b = 100$ km
0.1	20	2	2000	200
0.3	1	<1	90	10
1.0	≪1	≪1	3	<1

Note. Total number of impacts per square meter for apex hemisphere spacecraft flybys with impact parameters $b = 15$, 100 km. The first column gives the minimum detectable particle size.

4. DISCUSSION AND CONCLUSIONS

We have exploited the LDEX measurements at the Moon to model the dust ejecta from NEAs exposed to a near-identical impactor distribution. We found that the density of an NEA ejecta cloud can be scaled as $R^2a^{-2.7}$ for different sized targets and grain sizes for bodies near 1 au. The dust cloud distribution around asteroids near 1 au is predicted to be highly asymmetric, mirroring the local time dependence observed in the lunar dust cloud. The very same meteoroid sources that produce impact ejecta at the Moon are expected to produce comparable outbound ejecta flux distributions at asteroids near 1 au.

For objects that do not reside at 1 au, the impactor distribution may be significantly different. To extend this analysis to bodies at different heliocentric distances, such as objects in the asteroid belt, trojans, and the moons of Mars, for example, a more comprehensive study must be undertaken to understand the response of airless bodies to a large range of impacting distributions. However, for other airless bodies in the solar system that orbit the Sun, we expect the organization of the impacting population into the HE, AP, AH, and AA sources and subsequent ejecta distribution to be qualitatively similar to that described in this work.

The choice of mixing ratios used in this work represents a case that is symmetric about the apex direction. The various meteoroid sources have been observed to vary both in magnitude and direction (Campbell-Brown 2008; Szalay & Horányi 2016b). While the AP source was found to produce the most ejecta of all the sources, due to its large impact velocity, the HE and AH sources significantly govern the structure of the dust cloud. The dominance of the HE and AH sources may alternate throughout the year. Here we showed the symmetric case for the average asteroidal dust cloud. However, at any given time during the year, the ejecta cloud may be canted toward or away from the solar direction, the former being observed at the Moon during the months of 2013 October to 2014 April. In addition, we only considered the asteroids on circular orbits near 1 au. For eccentric orbits, the relative importance of each source may also depend on the target asteroid's true anomaly, as has been observed at Mercury (Marchi et al. 2005; Borin et al. 2016).

Though it is outside the scope of this study, meteoroid bombardment can release large quantities of neutrals from the surfaces of airless bodies (Cintala 1992). This has been observed both at the Moon (Verani et al. 1998; Smith et al. 1999; Colaprete et al. 2016; Szalay et al. 2016) and Mercury (Killen et al. 2010; Sarantos et al. 2011; Merkel et al. 2016). We expect a similar and asymmetric response for asteroidal surfaces, where a component of the neutral exosphere will be generated by high-velocity meteoroid impacts.

In addition to meteoritic bombardment, electrostatic effects may also contribute to ejection rates for very small asteroids. The existence of dust ponds on Eros, which were observed by the NEAR-Shoemaker mission, may indicate small-scale electrostatic mobilization (Hughes et al. 2008); however, the erosion of boulders has also been proposed as a mechanism for this unique phenomenon (Dombard et al. 2010). While no direct evidence of high-velocity electrostatic ejection was found at the Moon (Szalay & Horányi 2015b), recent laboratory measurements suggest that electrostatic forces can also eject a significant amount of grains off of surfaces. This process has been suggested to be most efficient on the lit hemisphere of an asteroid (Wang et al. 2016). An observed asymmetry of the dust density distribution near NEAs could also help to gauge the relative importance of dust mobilization and ejection due to impacts versus electrostatic effects.

Dust detectors can make valuable measurements near large asteroids ($R \gtrsim 10$ km), though we suggest flybys near smaller objects would yield negligible impact rates. These results can be used to optimize the encounter geometry of a future mission to an airless body to maximize the science return while minimizing the hazard due to dust impacts. In situ dust measurements at larger asteroids could garner valuable information about the local dust environment at 1 au. An in situ dust detector with chemical composition capabilities, or an aerogel dust capture experiment followed by the return of the samples to Earth, could greatly advance our understanding of the chemical makeup of these objects, and provide complementary data to confirm the conclusions of remote sensing spectral observations of these bodies.

LDEX data are available through NASA's Planetary Data System. M. Horányi was supported by the Institute for Modeling Plasma, Atmospheres, and Cosmic Dust of NASA's Solar System Exploration Research Virtual Institute. We thank Andrew Poppe, Juergen Schmidt, and Zoltan Sternovsky for insightful discussions on dust dynamics, and Shantanu Naidu for discussions on the population of asteroids near 1 au. The authors thank one anonymous reviewer for constructive comments.

REFERENCES

Borin, P., Cremonese, G., Bruno, M., & Marzari, F. 2016, Icar, 264, 220
Bottke, W. F., Morbidelli, A., Jedicke, R., et al. 2002, Icar, 156, 399
Campbell-Brown, M. D. 2008, Icar, 196, 144
Cintala, M. J. 1992, JGR, 97, 947
Colaprete, A., Sarantos, M., Wooden, D. H., et al. 2016, Sci, 351, 249
Dombard, A. J., Barnouin, O. S., Prockter, L. M., & Thomas, P. C. 2010, Icar, 210, 713
Elphic, R. C., Delory, G. T., Hine, B. P., et al. 2014, SSRv, 185, 3
Harris, A. W., & D'Abramo, G. 2015, Icar, 257, 302
Horányi, M., Sternovsky, Z., Lankton, M., et al. 2014, SSRv, 185, 93
Horányi, M., Szalay, J. R., Kempf, S., et al. 2015, Natur, 522, 324
Hughes, A. L. H., Colwell, J. E., & Dewolfe, A. W. 2008, Icar, 195, 630
Killen, R. M., Potter, A. E., Vervack, R. J., Jr, et al. 2010, Icar, 209, 75
Mainzer, A., Grav, T., Bauer, J., et al. 2011, ApJ, 743, 156
Marchi, S., Morbidelli, A., & Cremonese, G. 2005, A&A, 431, 1123
Merkel, A. W., Cassidy, T. A., Vervack, Jr., R. J., et al. 2016, Icar, 281, 46
Postberg, F., Grün, E., Horányi, M., et al. 2011, P&SS, 59, 1815
Sarantos, M., Killen, R. M., McClintock, W. E., et al. 2011, P&SS, 59, 1992

Smith, S. M., Wilson, J. K., Baumgardner, J., & Mendillo, M. 1999, GeoRL, 26, 1649
Szalay, J. R., & Horányi, M. 2015a, GeoRL, 42, 10580
Szalay, J. R., & Horányi, M. 2015b, GeoRL, 42, 5141
Szalay, J. R., & Horányi, M. 2016a, Icar, 275, 221
Szalay, J. R., & Horányi, M. 2016b, GeoRL, 43, 4893
Szalay, J. R., Horányi, M., Colaprete, A., & Sarantos, M. 2016, GeoRL, 43, 6096
Verani, S., Barbieri, C., Benn, C., & Cremonese, G. 1998, P&SS, 46, 1003
Wang, X., Schwan, J., Hsu, H.-W., Grün, E., & Horányi, M. 2016, GeoRL, 43, 6103
Westphal, A. J., Snead, C., Butterworth, A., et al. 2004, M&PS, 39, 1375